

Characterization of a fiber laser hydrophone for acoustic neutrino detection

E. J. Buis^{a,b,*}, A. M. von Benda-Beckmann^a, E. Doppenberg^a, J. Dorant^a, T.H. Jansen^a,
P. Toet^a, P. Verhooren^a, J. de Vreugd^a

^a*TNO, Netherlands Organisation for Applied Sciences, Delft, The Netherlands*

^b*Nikhef, National Institute for Subatomic Physics, Amsterdam, The Netherlands*

Abstract

This paper presents the development and characterization of a fiber laser hydrophone designed for deep-sea applications, with a focus on detecting neutrino interactions via their acoustic signatures. The hydrophone design includes a static pressure compensation mechanism, ensuring reliable operation at depths exceeding 1 km. The performance of the hydrophone was evaluated through laboratory tests and experiments in an anechoic basin, where its transfer function was measured before and after a 140-bar pressure cycle. The results show that the hydrophone maintains its sensitivity, with resonance peaks identified in both low- and high-frequency ranges. The hydrophone's sensitivity to acoustic signals was also compared to ambient sea state noise levels, demonstrating compatibility with the lowest noise conditions.

1. Introduction

In the search for ultra-high energy neutrinos alternative detection techniques are being pursued. One of them is the detection of neutrino interactions through their acoustic signature in the deep sea [1, 2, 3]. This method benefits from the relatively long attenuation length of the sound in water, allowing to establishment of an acoustic neutrino telescope with a large detection volume with a relative sparse network of hydrophones. Still, for an acoustic telescope to observe the small predicted flux of ultra high energy neutrinos, the hydrophones are required to be sensitive enough to detect the weak signals induced by neutrino interactions. In addition, a neutrino telescope will consist of a large number of hydrophones.

Given the large number of hydrophones required for an acoustics neutrino telescope in combination with the required sensitivity, a promising technology is the fiber laser hydrophone technology as it combines sensitivity with a relative simple and cost-effective method of deployment. Fiber optic hydrophones (and fiber optic sensing) have been discussed in detail in literature. For scientific objectives additional requirements have to be met on the performance of the hydrophones, such as the operation in the deep-sea environment (> 1 km deep), sensitivity (comparable to the lowest sea state noise levels, SS0-SS1) and large operating frequency bandwidth (> 10 kHz). The anticipated acoustic signals vary with neutrino energy but are typically just

*ernst-jan.buis@tno.nl

above the sea state noise, with signal amplitudes ranging from 10 to several hundred millipascals [4, 5].

In this paper we discuss the design of a new version of a hydrophone transducers that follows the design concepts based on the fiber laser technology as we have described previously [6, 7]; this time we focus on introducing a static pressure compensation mechanism. We present the results of an extensive set of measurements to characterize the new hydrophone transducer and to qualify for operation in the deep sea. The outline of this paper is as follows. In the next section we discuss the fiber hydrophone technology and the design of the transducer in particular. Then in section 3 we detail the experimental set-up after which we show the results of the characterization measurements. We summarize in section 6.

2. Hydrophone concept design

The concept of fiber hydrophone relies on the measurement of a wavelength shift in an optical fiber that is induced by sound pressure in water. A pressure wave will be converted to a wavelength shift by a transducer that is glued onto the fiber. The sensitivity of the hydrophone technology is determined by the performance of the transducer to efficiently convert pressure into strain in the optical fiber, but also of the optical fiber to convert strain into a wavelength shift. The wavelength shift is determined using a dedicated interferometer. The interferometer is a central part of the complete readout system. When designing and characterization of the hydrophone technology, as discussed in this paper, all three components have been investigated.

2.0.1. Transducer design

The transducer is in-house designed and is shown in figure 1. The design relies on one (or two) membranes placed on a cylindrical shaped housing. The hydrophone as shown in figure 1 is a cylindrical shaped transducer with a 250 μm thick membrane on the end of this cylinder. The dimensions of the membrane are determined by COMSOL and determines the position of the first mechanical eigenfrequency. The value of the eigenfrequency determines to first order the dynamical frequency range of the hydrophone. In the design a trade-off has to be made between the sensitivity and the dynamical range of the hydrophone.

A fiber is threaded through the membranes and glued. Particularly for this transducer, a hydrostatic pressure mechanism was introduced by an orifice in the housing, because the hydrophone is required to operate in the deep-sea and therefore to withstand high ambient pressure. The orifice allows water or oil to flow into the transducer to counterbalance the high pressure environment. Note however that a hydrophone with hydrostatic pressure compensation is expected to be less sensitive than an air-backed hydrophone. However, for an application in the deep-sea an air-backed volumes does not provide a solution, because the air is (completely) compressed by the ambient pressure.

The length of the transducer, i.e. 22 mm, is chosen to match the length of the fiber laser cavity (next section). The transducer is made of stainless steel, which is chosen because of its stiffness, density and ease of manufacturing. Then, two versions of the transducers have been produced: i) one membrane on one side of the cylinder as depicted in figure 1 and ii) with a membrane on each side on the cylinder. Fabrication and integration of the transducer was done at TNO. The membrane was laser-beam welded (LBW) on to the cylinder, while the orifices were

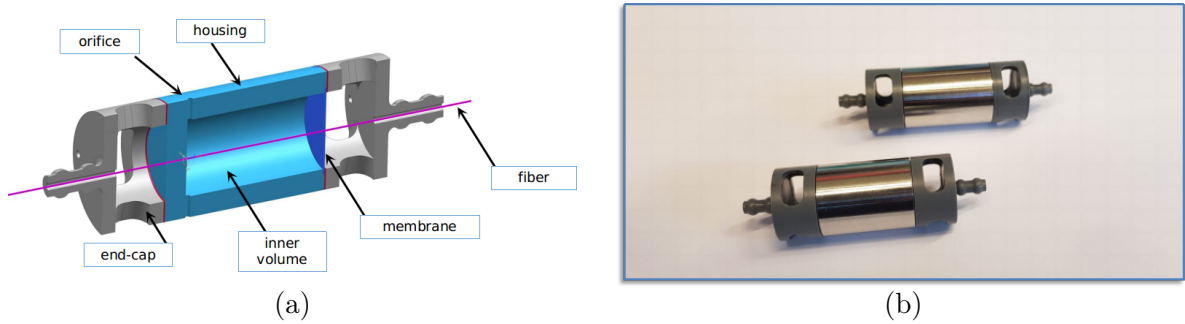


Figure 1: (a) The design of the fiber laser hydrophone, while in (b) a photo of two assembled hydrophones are shown. In (a) the concept of a single membrane hydrophone is shown.

EDM-drilled. The fiber was integrated in the transducer and glued on the membrane with glue (Loctite[®] EA9313). The fiber was not stripped from its coating before gluing. The pre-tension that was applied on the fiber amounted to about 0.1 N. Finally, to increase the robustness two end-caps are glued on either side of the cylinder to guide the fiber and to reduce the chance of breaking it.

2.1. Optical fiber hydrophone concept and signal formation

Dedicated optical fibers are realized that include a fiber laser as depicted in figure 2. The gain medium of the fiber laser is provided by the Erbium that is inserted, while the fiber Bragg grating (FBG) confines the laser cavity.

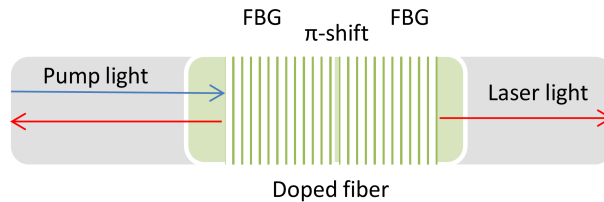


Figure 2: Schematic of a (distributed feedback) fiber laser.

The concept of a fiber laser hydrophone is based on the fact that deformation (or strain) of the fiber laser cavity will result in a shift of the emitted laser wavelength. This change of wavelength can then be sensed using an interrogator, which is connected to the optical fiber. In order to increase the sensitivity of the hydrophones a transducer is placed around the fiber laser to convert pressure in strain in the laser cavity. An important parameter in the design of a transducer is the *strain sensitivity*, which is the amount of pressure that is converted to strain (ε) and is usually given in units $n\varepsilon/\text{Pa}$.

For the discussion on strain sensitivity it is illustrative to discuss the strain dependence of the Bragg wavelength. As mentioned above the strain (ε) in the fiber induces a wavelength shift

($\Delta\lambda_B$) which can be described by [8]:

$$\Delta\lambda_B = (1 - p_e)\lambda_B\varepsilon \quad (1)$$

where p_e is an effective photo-elastic coefficient:

$$p_e = \frac{n}{2}(P_{12} - \mu(P_{11} + P_{12})) \quad (2)$$

Here P_{ij} are the Pockels coefficients of the optical fiber, n is the index of refraction and μ is the Poisson's ratio. Given the values of $p_e \sim 0.22$ and $\lambda_B \sim 1550$ nm, the wavelength shift dependence on the strain is given by:

$$\frac{\Delta\lambda_B}{\Delta\varepsilon} = 1.2 \left(\frac{pm}{\mu\varepsilon} \right) \quad (3)$$

As we will discuss in section 3, the hydrophone is read out using an unequal-arm interferometer in which phase difference between light from the different arms is determined by introducing an optical path difference (OPD) in two arms. This phase difference (ϕ) is defined as:

$$\phi = \frac{2\pi}{\lambda} \text{OPD} \quad (4)$$

where λ is the laser wavelength. A change in the central wavelength of the fiber laser induces a phase difference, which depends on the central wavelength and is given (for small wavelength changes) by:

$$\frac{\Delta\phi}{\Delta\lambda} = \frac{2\pi}{\lambda^2} \text{OPD} \quad (5)$$

The expressions as given in equations 5 and 3 are used to convert the measured phase to the strain in the fiber laser. The value OPD should be corrected for the index of refraction, i.e. the OPD in this case is n times larger than the physical length of the difference in the armlength, where n is the index of refraction of the glass fiber. In principle a larger OPD provides a higher sensitivity, but large armlengths in the interferometer are unpractical and susceptible for additional (internal fiber) noise. It was found that in our experimental set-up the optimal optical path difference was between 4 and 10 meter.

The fiber laser consists of a 22 mm long Erbium-doped Distributed Feedback Laser (DFB) produced by Exail. The length of the fiber laser is important and should be as short as possible to induce the maximum strain for the same pressure wave. Furthermore, the length of the transducer housing is matched to the length of the fiber laser.

3. Experimental setup

3.1. Interrogator

The read-out system of the fiber hydrophone is shown in figure 3 and consist of three main components. First, a pump laser is used to pump the fiber laser. The pump laser wavelength can be either 980 or 1480 nm. Here we use 980 nm.

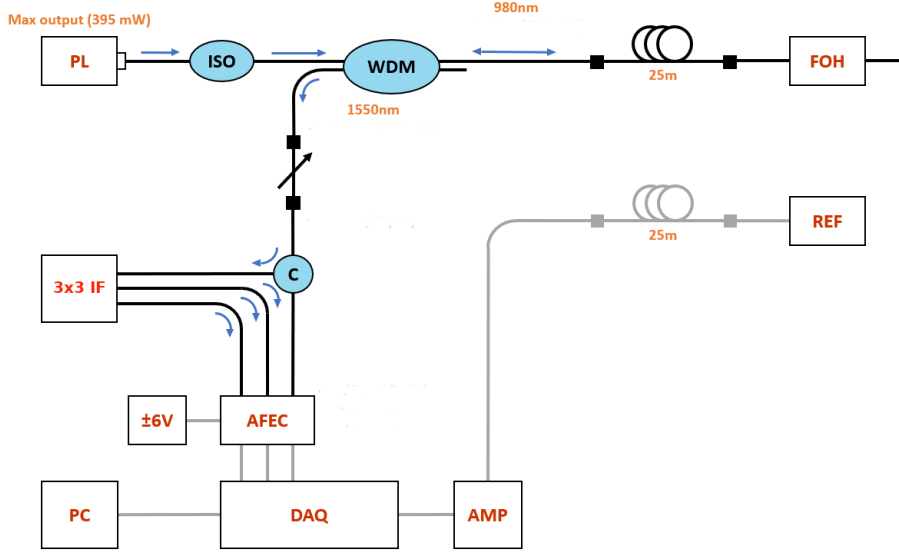


Figure 3: Schematics of the read out of a fiber laser hydrophone. Several abbreviations are used in the drawing: PL = pump laser; ISO = isolator; WDM = wavelength division multiplexer, FOH= fiber optic hydrophone; REF = reference hydrophone; IF = interferometer; C = circulator; AMP = amplifier; AFEC = Analog Front-End Controller

Secondly, an interferometer is used to determine the wavelength shift of the fiber laser light. We use a custom built interferometer for this based on a standard 3x3 coupler. While the input of the interferometer consists of three inputs, we only used two arms in the interferometer. A fixed and predetermined optical path difference (OPD) in the two arms has been chosen. The output of the 3x3 coupler consists of three light intensities (I_x) as indicated in figure 3. The outputs of the three arms are identical, but each is shifted in phase over $\frac{2}{3}\pi$. In addition, each intensity depends on the optical path difference as defined in the equation 6.

$$\begin{aligned}
 I_S &= I_0(1 + V \cos(\frac{2\pi}{\lambda} \text{OPD})) \\
 I_+ &= I_0(1 + V \cos(\frac{2\pi}{\lambda} \text{OPD} + \frac{2\pi}{3})) \\
 I_- &= I_0(1 + V \cos(\frac{2\pi}{\lambda} \text{OPD} - \frac{2\pi}{3}))
 \end{aligned} \tag{6}$$

where I_0 is the normalized amplitude of the signal and V is the visibility. Using the phase shift and the intensity of each arm, the optical path length (OPD) is given by the following equation:

$$\phi = \arctan\left(\frac{\sqrt{3}(I_+ - I_-)}{2I_S - I_+ - I_-}\right) \tag{7}$$

$$\text{OPD} = \frac{\lambda}{2\pi} \arctan\left(\frac{\sqrt{3}(I_+ - I_-)}{2I_S - I_+ - I_-}\right) \tag{8}$$

Because the optical path difference (OPD) is known, the wavelength shift of each hydrophone in the string can be accurately determined when the three output intensities are measured.

Then, thirdly, we convert the 3 optical signals from the interferometer arms into a digital signal. To do so we collect the light intensities from the interferometer using standard commercial available photo-diodes and converted using a 24-bit ADC at a sample rate of 200 kHz. Finally, we use the same DAQ system to register the signals from a commercial available reference hydrophone (section 3.3).

3.2. Phase measurement calibration

As discussed above the transducer will convert pressure waves into strain, resulting in a wavelength shift emitted by the fiber laser. We use a 3x3 interferometer to determine the wavelength shift, by measuring the phase shift that the change of wavelength introduces. To accurately determine the phase shift, we calibrate the output of the three arms of the interferometer. In figure 4 (a) we show the output of the three interferometer arms as a function of time that is used to determine the phase. At certain moments in time we apply strain on the one the arms, which is large enough to exert phase shifts larger than 2π radians. From these fringes, we can then correct the gain and phase of each arms in the offline analysis. The resulting phase as a function of time is shown in figure 4 (b).

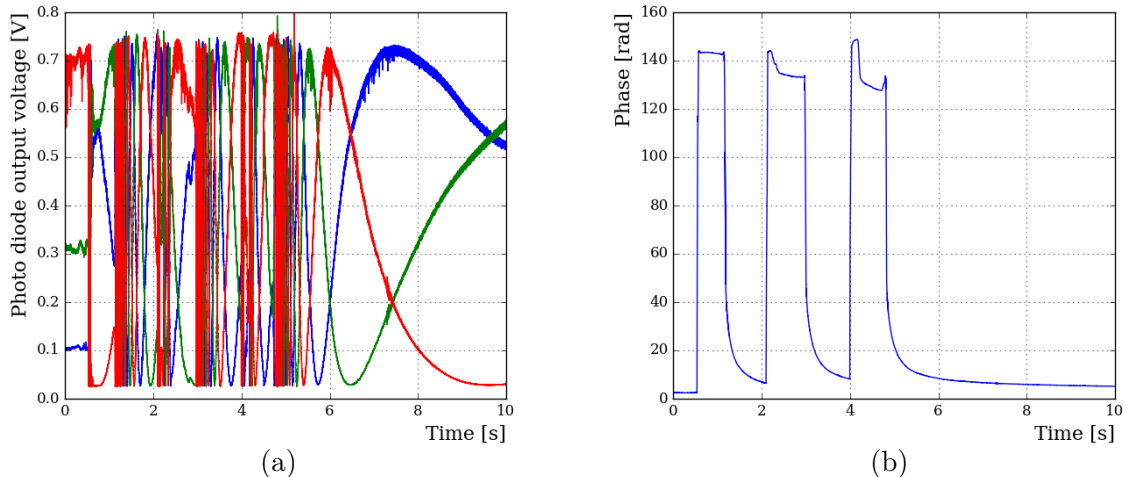


Figure 4: (a) The output of the three arms as a function of time. At three moments in time, strain is applied on of the arms in the interferometer, large enough to induce a phase shift of more than 2π radians. In (b) the resulting phase shift is shown as a function of time.

3.3. Acoustic setup

To characterize the fiber hydrophone, the experimental setup and the hydrophones as described above were taken to the anechoic basin at the TNO laboratories. The experimental set-up in the basin is depicted schematically in figure 5. The basin it self measures $8 \times 8 \times 10 \text{ m}^3$. Two projectors were used: i) an ACTRAN projector (type LFPX-4), which provides acoustic signals for the lower frequencies and ii) an ITC 1042 projector which provides an acoustic source at higher frequencies, i.e. above 10 kHz.

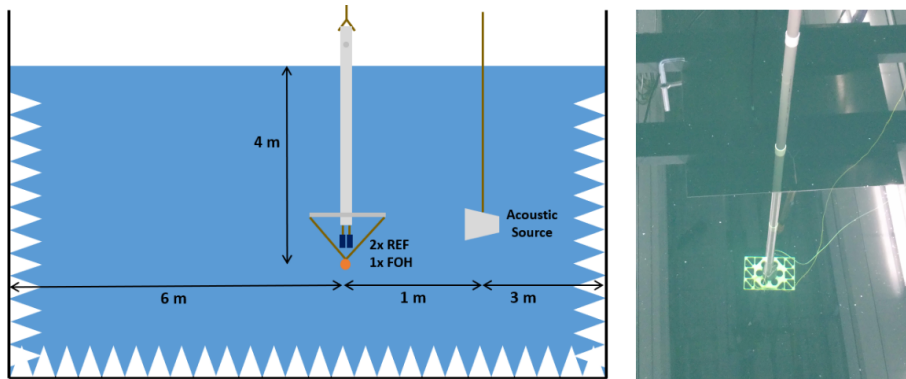


Figure 5: The left panel shows a schematic of the acoustic measurement setup in the anechoic basin. The right panel displays a photograph of the mechanical support structure, to which both the fiber hydrophone and the reference hydrophone are attached.

A mechanical support structure was produced to which both the fiber hydrophone and the reference hydrophone are attached.

3.4. Pressure calibration

The calibration of the fiber optic hydrophone is established using the reference hydrophone, i.e a commercial available Bruel & Kjaer BK8103. In turn this hydrophone is calibrated using a pistonphone (type BK4229 with coupler UA 0548), which provides a well-defined signal at 250 Hz to the coupled reference hydrophone. This signal has been calibrated and provides a well defined signal of 166 dB re μPa to the reference hydrophone. The response of the BK8103 is specified to be flat up to 50 kHz, so that the calibration of the reference hydrophone is valid for the range at which the fiber optic hydrophone is tested.

4. Measurement results

4.1. Hydrophones under test

To assess the performance of the hydrophones a number of different configurations have been integrated and characterized. In table 1 the various hydrophone configurations are listed. Each of the hydrophones have been characterized, but in addition we performed a number of measurements to better understand the impact of several issues during integration. One hydrophone has been subjected to a qualification measurement.

All hydrophones were filled with water. To properly fill the volumes within the transducers, an experimental set up was made to fill the transducers without air bubbles. After integration the transducers were put in a reservoir under vacuum and water was led in the reservoir. This controlled way of filling ensured that the amount of air in the volumes after being filled was minimal.

| Configuration | Remarks |
|-----------------|---------------------------------|
| Single membrane | with and without cap |
| Single membrane | with and without air bubble |
| Double membrane | before and after pressure cycle |

Table 1: Devices integrated for characterization.

4.2. Noise

Prior to the integration of the fiber laser hydrophones, bare fiber lasers coupled to the interrogator have been characterized. Using the interrogator the phase noise of the fiber laser without an transducer attached to it has been determined in an acoustically insulated environment and free from vibrations. In figure 6 the wavelength noise for one of the fiber lasers is shown for as a function of the frequency. In comparison we show the noise measurement of an acoustic insulated fiber laser. While the packaged hydrophone was read out using an interferometer with a OPD of 4 m, the measurement on the fiber laser was carried with an interferometer with an OPD of 10 m. In addition, the fiber laser was kept in an acoustically isolated block of aluminium, free from vibrations. Hence, the measurements on the bare fiber laser presents the noise floor of the interrogator. As can be seen from the figure, the noise level of the integrated and the bare fibers do not differ much at higher frequencies, i.e. above 1 kHz. At a frequency of 10 kHz, the difference in the noise level is about 2 dB. At lower frequencies the integrated fiber pick up acoutic and vibration noise. Spikes that appear in the noise spectra originate from electromagnetic interference.

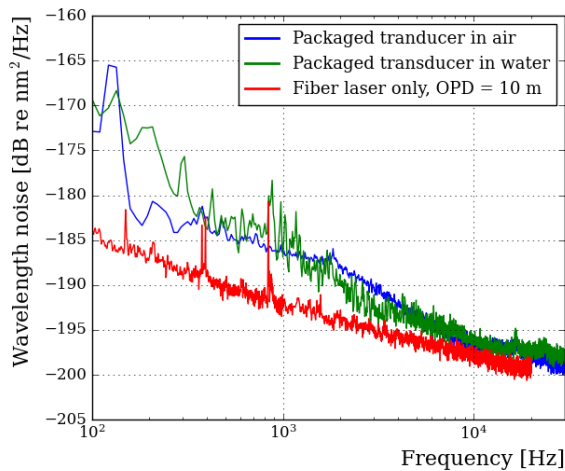


Figure 6: Power spectral density of the phase noise of a fiber laser integrated in an optical fiber hydrophone compared to the noise of an acoustically insulated bare fiber laser.

4.3. Time trace and Bode diagram

The fiber hydrophone was calibrated and deployed in the acoustic basin as discussed in section 3 and depicted in figure 5. One of the basic measurements is a frequency sweep in which the output is measured from both the fiber hydrophone and the reference hydrophone. The result from one such sweep is plotted in figure 7. The upper panel shows the spectrogram of the output of the fiber hydrophone. A clear increase of the acoustic frequency from 200 Hz to 20 kHz in the blue and purple band. In addition, the spectrogram shows some of the overtones at twice the nominal frequency in a dim blue band. It was found that these overtones originate mainly from harmonic distortions of the input amplifier of the projector.

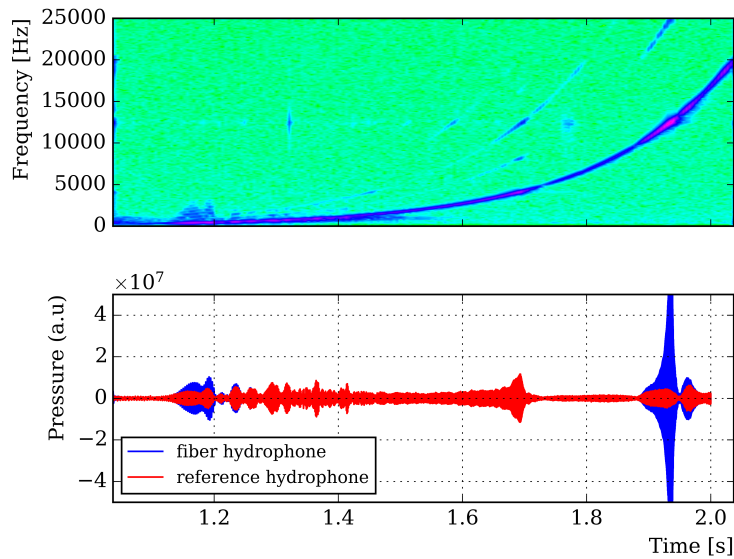


Figure 7: Example spectrogram of a single membrane fiber hydrophone (top panel) and time traces from the fiber and reference hydrophones (bottom panel) in a frequency sweep measurement.

In the lower panel of figure 7 the time trace for both the fiber hydrophone and the reference hydrophones are shown. Here, we present the uncalibrated data to demonstrate that (i) the output of the projector, as recorded by the reference, is not flat across the spectrum, and (ii) the transfer function of the fiber hydrophone is also not uniform, but rather complex. It shows the importance of the reference hydrophones in these measurements to correct for the distortions in the source and the investigate the transfer function of the fiber hydrophone.

Frequency sweeps were used to determine transfer functions and were plotted in general Bode diagrams consisting of a Bode magnitude plot and a Bode phase plot. In addition we determine the coherence between the signals in the fiber hydrophone and the reference hydrophone. The coherence confirms whether the measured signals is observed in both hydrophones and hence whether the input is of acoustic origin. We compute (magnitude of the) transfer function (T_{xy})

and the coherence (C_{xy}) according:

$$T_{xy}(f) = \frac{|S_{xy}(f)|}{S_{xx}(f)} \quad (9)$$

$$C_{xy}(f) = \frac{|S_{xy}(f)|^2}{S_{xx}(f)S_{yy}(f)} \quad (10)$$

where $S_{xy}(f)$ are the cross-spectral density between fiber hydrophone and the reference hydrophone, and $S_{xx}(f)$ and $S_{yy}(f)$ the auto spectral density of fiber and reference hydrophone respectively. Furthermore, the phase in the Bode diagram is defined as the angle between input of at the reference hydrophone and fiber hydrophone.

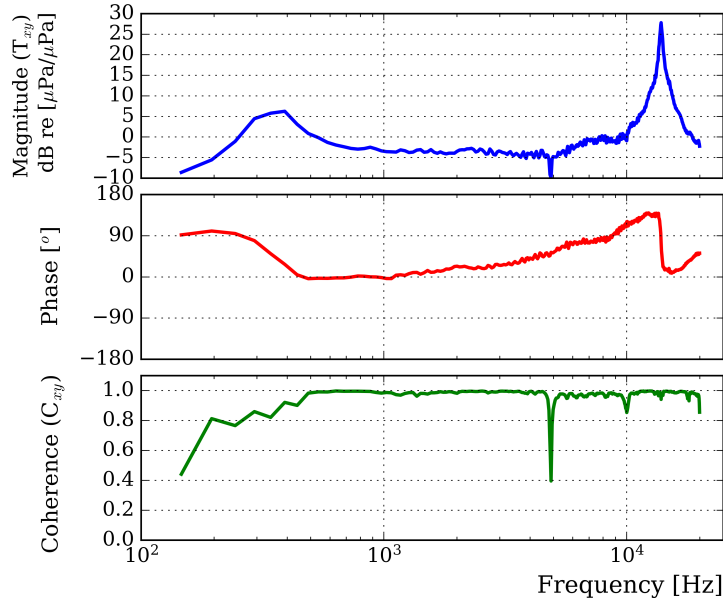


Figure 8: Response of a single membrane hydrophone to a sweep signal with a frequency between 200 Hz and 20 kHz. In the top panel the Bode magnitude plot is shown; in the middle panel the Bode phase plot is shown, while the bottom panel shows the coherence of the signal between the fiber optic hydrophone and the reference hydrophone.

In figure 8 we show the Bode plot of a frequency response measurements in which an acoustic frequency sweep between 200 Hz and 20 kHz was offered to both the (double membrane) fiber hydrophone and the reference hydrophone. The panels in this figure show (from top to bottom) the magnitude and the phase of the transfer function as well as the coherence (cross spectral density) between the fiber hydrophone and the reference. The coherence in the frequency range of 200 Hz - 20 kHz is on average high, albeit that there are several dips, which can be attributed to non-acoustic signals such as electronic noises.

The transfer function shows several features as shown in figure 8. At low frequencies, i.e. below ~ 600 Hz a resonance peak can be found, which is a Helmholtz resonance due to the small orifices in the transducer. When the orifices were closed off using a piece of tape, the Helmholtz resonance disappeared. At higher frequencies, i.e. above 10 kHz a peak in the transfer function appears, which is the first eigenfrequency and is due to a mechanical resonance. At the position of the resonance peaks, a phase jump is shown in the Bode phase plot in the middle panel.

Bode plots are used to determine the strain sensitivity of the transducer. From the measured laser phase shift (and hence wavelength shift) the strain sensitivity can be determined using equation 3. In figure 9 we show the strain sensitivity for both the single and double membrane hydrophones. The sensitivity is given for the frequency range in which a frequency sweep has been carried out and in which the coherence is sufficient (i.e. $C_{xy} > 0.7$). As we characterized two single membrane transducers, we compared their transfer functions, and no significant differences were found.

In addition the sensitivity as predicted by the COMSOL finite element analysis is given. As can be seen from the figure, the measured strain sensitivity matches reasonably with what has been determined using the design software, albeit that the position of the resonance peak is found at lower frequencies than what has been designed.

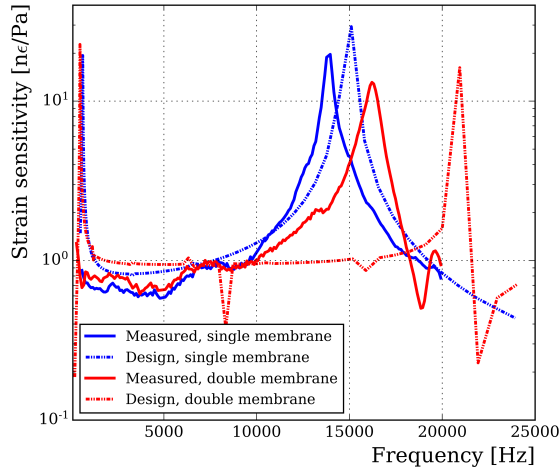


Figure 9: Measured and designed strain sensitivity of a single and double membrane hydrophone as a function of the frequency.

4.3.1. Impact of protective cap

As shown in figure 1 a cap is glued on both ends of the transducer to guide the fiber through the membrane of the transducer. The cap was added to the transducer for practical reasons, to avoid breaking the optical fiber during a extensive set of measurements and handling. To determine the impact of the cap on the acoustic characteristics of the hydrophone, the transfer

function of the hydrophone has been determined with and without the cap. In figure 10 (a) the transfer function of the single membrane sensor is shown for both configurations. As can be seen from the figure, the cap has a non-negligible impact on the acoustic characteristics: the main mechanical resonance has shifted to a lower eigenfrequency. In addition, a second resonance peak can be seen that is absent when no cap has been applied. The main mechanical resonance peak shifts from 13.9 kHz to a frequency of 12.0 kHz. Furthermore there are two small anti-resonance peaks, at 4.8 and 5.7 kHz respectively. The latter is introduced by the cap and shows directionality, while the first anti-resonance peak is always present, irrespective of the cap or direction w.r.t to the sound source. The origin of the peak is unknown. Note further that the Helmholtz resonance peak remained at its position.

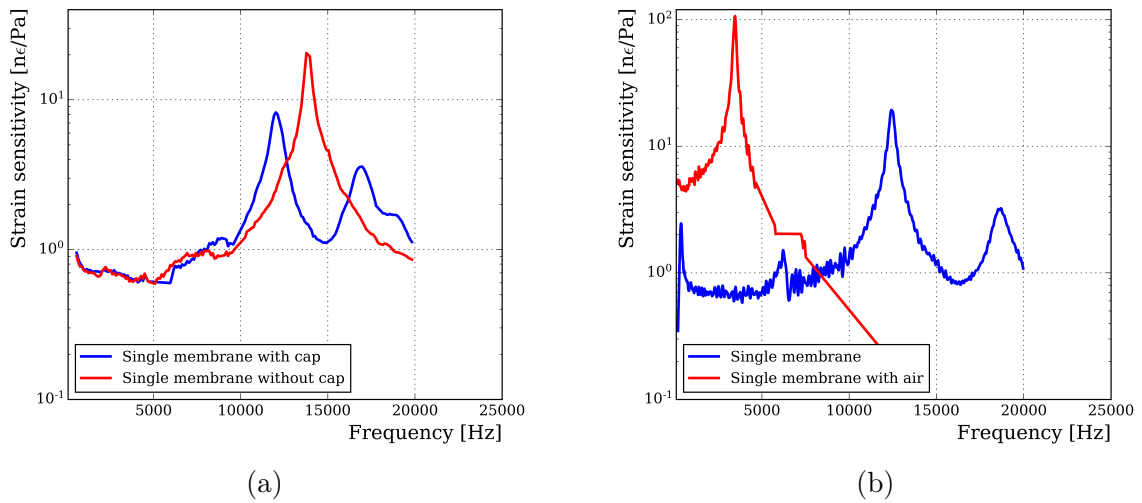


Figure 10: (a) The hydrophone response as a function of the acoustic frequency for a single membrane transducer with a cap compared to a single membrane transducer without a protective cap. In (b) the transfer functions of a sensor with a sensor volume completely filled with water and with an air bubble inserted.

4.3.2. Air bubbles in the sensor

As mentioned in section 2.0.1, a static pressure mechanism has been implemented by introducing two orifices in the sensor. Prior deployment the sensor volume has been filled with water, which allows to withstand the ambient pressure when the sensor is required to operate at large depth. Filling the sensor volume with water however, (instead of air) does compromise the sensitivity of the sensor. It is important to completely fill the sensor as any residual air will provide a risk to deform and damage the sensor. It is anticipated that residual air is expected to have an impact on the transfer function. To verify the impact of air in the sensor, we have determined the transfer function without air, after careful filling of the sensor and with air. Then, a small bubble of air was inserted in the sensor using an injection needle. Unfortunately we did not have full control of the size of air bubble, but we estimated its size to be small and around 1% percent in volume only with respect to the sensor volume.

In figure 10 (b) we show the transfer function with and without air bubble in the sensor. Comparing the transfer functions differ both in the position of the mechanical resonant frequency as well as the overall strain sensitivity. After introducing air in the sensor volume, the peak shifts to lower frequencies and the overall sensitivity seem to increase. The shape of the transfer function did not change. The impact of the air bubble is confirmed by simulations.

4.4. Linearity

To check the linearity of the response of the hydrophone the response was determined to a tone of 5 kHz at several setting of the sound source. The sound pressure level of the source was set by a voltage and the recorded pressure level was determined for a single tone of 5 kHz. In figure 11 the recorded height of the tone as a function of the voltage applied to the source is shown. The sensor shows an excellent linear behaviour in the applicable range.

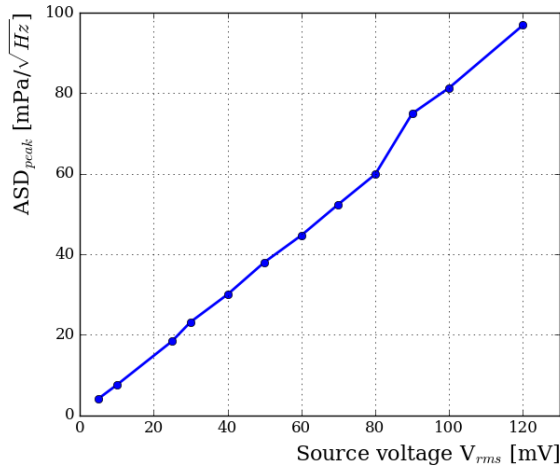


Figure 11: Linearity of a single membrane sensor.

4.5. Directionality

The experimental set-up allowed to change the orientation of the fiber hydrophone with respect to the source, so that the directionality could be determined. To do so, the transfer function has been determined at various functions for both types of hydrophones. In figure 12 we show the transfer function for various angles with respect to the source for a double membrane sensor. As can be seen from the figure, the transfer function for the double membrane hydrophone varies with the angle, while for the single membrane hydrophone the effect is less pronounced. We furthermore observe that the direction sensitivity is not observed outside the resonance peak. The position of the resonance peak is independent of the angle of incidence.

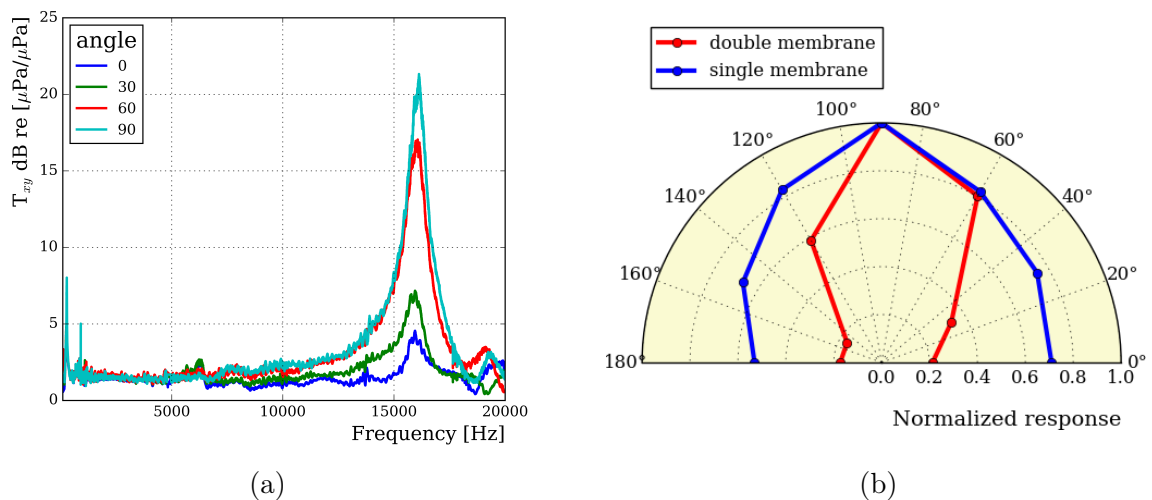


Figure 12: Directionality of the response. In (a) the transfer function for a double sensor membrane is shown for various angles of the sensor w.r.t. the source. In (b) the resonance peak (normalized to the 90° response) is shown for two types of sensors as a function of the incident angle.

4.6. Pulse measurement

The investigation of the (complex) transfer function of the fiber hydrophone is justified when we have a look at the single pulses or transients. A number of pulse trains have been recorded to this end. In figure 13 we show an example of one such pulse, measured with both the fiber hydrophone. The impact of the resonant peak is apparent as the signal as measured using the fiber hydrophone shows a large amount of ringing. Knowing the transfer function of the hydrophone, we can deconvolute the transfer function as compare the resulting pulse with the reference hydrophone. To do so we take the transfer function as shown in figure 8 and do interpolation to match the transfer function to the amount of data points in the pulse. The result of the deconvolution is shown in the insert of figure 13. After deconvolution, both pulses are nearly indistinguishable, an indication that the transfer function function has been properly determined. Note that also the reference hydrophone shows some ringing. As the reference hydrophone has a flat frequency response, the ringing is assumed to originate from the source.

4.7. Pressure stress tests

One of the challenging requirements to meet is the fact that the hydrophones is operated in the high pressure environments of the deep sea. A first investigation to verify the compliance with the requirement has been carried out in a pressure stress test. To this end a hydrophone was placed in a small hyperbaric pressure vessel and put under pressure of 140 bar. The pressure was applied at several steps. In figure 14 the time line of the measurement is shown: during a time period of 600 seconds the phase measurement in the interferometer has been monitored, while the ambient pressure increased by steps of roughly 20 bar. The pressure was applied manually (pump HP32-8 by Uraca) in steps of roughly 20 bar, while each step was followed by a few

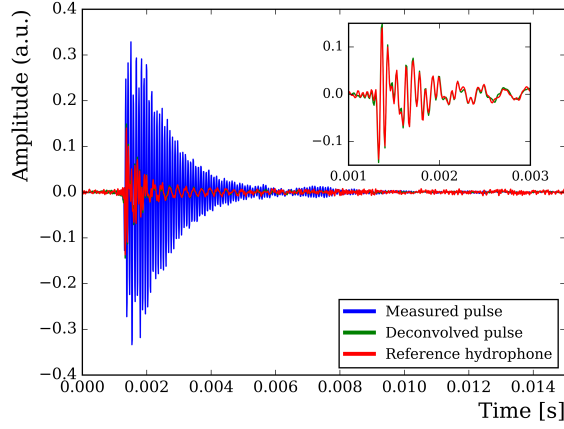


Figure 13: Measurement of a single pulse using both the fiber hydrophone and the reference hydrophone. In addition we show the deconvoluted pulse as measured using the fiber hydrophone.

seconds of stable pressure until a maximum of 140 bar was reached. Then, the pressure was held to a constant level for about 3 minutes after which the pressure was released and returned to ambient pressure. The graph in figure 14 shows the wavelength shift during the complete pressure cycle. Note that the maximum pressure applied was limited by the fact that the vessel was put under pressure by hand.

The high pressure will slightly deform the transducer and the integrated fiber laser. This gives rise to a phase shift as measured in the interferometer in the interrogator and is plotted in figure 14. Subsequently the wavelength shift of the fiber laser has been determined using equation 5. The figure shows that due to the deformation of the transducer the shift of the central wavelength of the fiber laser will shift 60 pm at a pressure of 140 bar. Once the hydrophone will be deployed to the deep sea, the central wavelength of the laser will remain at this value. Note that this measurement indicates that the pressure compensation does not remove the dependency of the wavelength of the hydrophone on the applied depth completely, but enough for proper operation.

If we zoom in on the time trace of the measurement of the phase (and hence the wavelength) during the pressure qualification as shown in figure 14, then we can plot again the spectrogram. The spectrogram of the period between 354 and 357 seconds after the start of the measurement is shown in the figure 15. In the top panel we show the spectrogram, while in the bottom panel the time trace is plotted. The time trace is plotted after a high-pass filter (with a cut-off frequency of 500 Hz). The time trace shows spiky behaviour: The measured wavelength does not only show a gradual decrease and subsequent increase during the measurement (as shown in figure 14), but additional transient signals have been recorded. The origin of the signal is not clear; this could well be the deformation of the transducer, but also acoustic signals from the pressure vessel itself. We can use these transients to investigate one of the main features of the transfunction, i.e. the

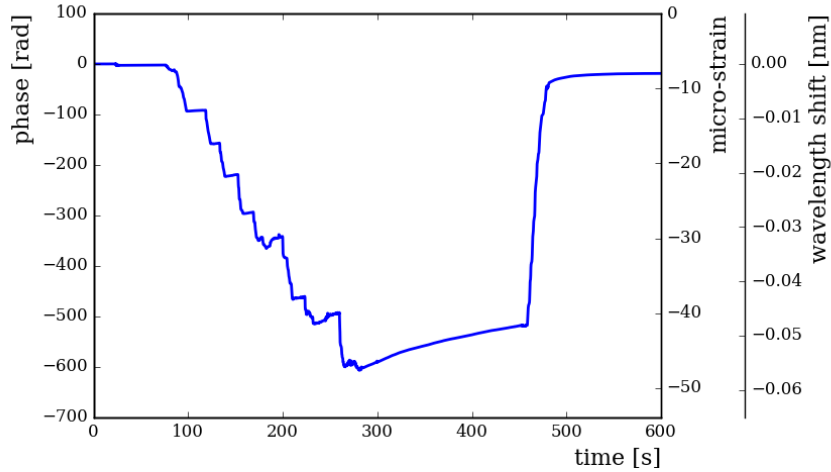


Figure 14: Measurement of the phase change during a pressure cycle. The pressure increases in steps of roughly 20 bar up to a maximum of 140 bar.

resonance peak. The spectrogram shows the position of the resonance peak at ~ 16 kHz by the dark blue horizontal band. We can therefore conclude that the position of the resonance peak did not alter when the transducer was put under a static pressure of 140 bar.

A measurement of the transfer function was carried out before and after the pressure cycle in the anechoic basin of which the results. There was no noticeable difference found between the two transfer functions: The mechanical resonance peak was found at the same frequency and the overall strain sensitivity remained identical. This indicates that the sensor and the attachment of the fiber to the transducer did not deform. In addition, the same directionality has been found as depicted in figure 12.

It should be noted that the pressure cycle in this experiment was much shorter than what can be expected during deployment in the applicable environment. In case the hydrophones would be deployed in the deep sea, the rate of pressure change would be an order of magnitude smaller, i.e. the hydrophone would experience a more benign change of environment.

5. Sensitivity

Based on the measured transfer function and system noise, it is possible to determine the sensitivity of the fiber laser hydrophone. To do so we take the strain sensitivities as shown in figure 9 of the two types of transducers and the system noise as depicted in figure 6. The resulting sensitivity of the hydrophone as a function of the acoustic frequency is plotted in figure 16. It is illustrative to compare the sensitivity with the noise levels as expected in the deep sea. It is common to express the deep sea noise in terms of a sea state noise ([9]), which runs from sea

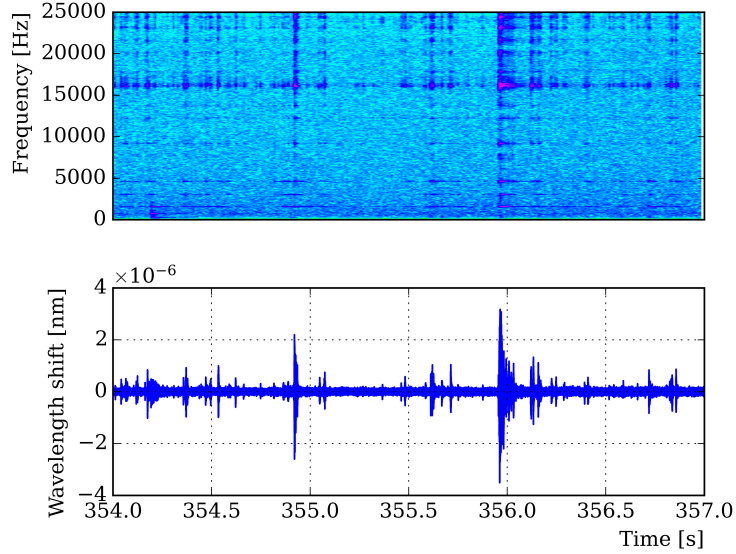


Figure 15: Spectrogram (top) and time trace (bottom) of a brief event recorded during the pressure test.

state 0 (SS0) to SS9. The expression of the sea states is provided in [10, 11] and is given by:

$$P(f, n_s) = 10 \log_{10}(f^{-\frac{5}{3}}) + 30 \log_{10}(n_s + 1) + 94.5 \left[\text{dB re } \frac{\mu\text{Pa}^2}{\text{Hz}} \right], \quad (11)$$

where f is the frequency and n_s the sea state.

Some levels have been depicted in figure 16 as well and it can be concluded that the overall sensitivity compares to the lowest expected noise levels in the deep sea, varying between sea state 0 and 1. In particular, the sensitivity is enhanced down below sea state 0 at the position of the resonance peaks. Note further that the sensitivities of the two type of hydrophones are comparable away from the resonance peaks. Furthermore, although not shown in the figure, the response of the hydrophones is non-zero well above 20 kHz, which allows for higher frequency signals to be detected.

6. Conclusions

This paper presents the development of a highly sensitive hydrophone sensor utilizing fiber laser technology, designed for potential use in future acoustic neutrino telescopes. To meet the demands of deep-sea operation, the sensor must function at ambient pressures of at least 10 MPa while detecting transient pressure signals in the range of several mPa. A pressure compensation mechanism has been implemented to offset static pressure levels.

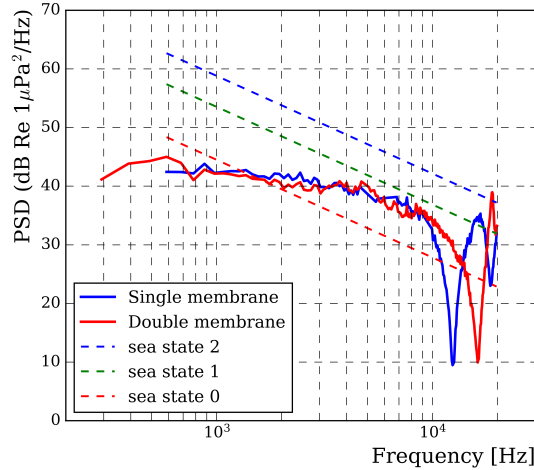


Figure 16: Sensitivity of the two tested types of fiber hydrophones as a function of frequency. In addition ambient sea state noise levels are drawn for comparison. See text for details on sea state noise.

The hydrophone system has been subjected to a detailed investigation of the acoustic performance. A dedicated set up in an anechoic pool has been made for this purpose. Based on the presented results we arrive at the following conclusions. The transfer function of the hydrophone follows the predictions of the finite element analysis that were carried out during the design phase: Two resonance peaks are found in the response of the hydrophone: i) one Helmholtz resonance at lower frequencies (< 500 Hz) and ii) one mechanical resonance of the transducer well above 10 kHz. The exact values of the eigenfrequencies differ from the predicted values, but the dynamical range of the sensors is found to be 200 Hz to 20 kHz, compliant with the main frequency components of a transient neutrino signal.

There is significant difference between the transfer functions of a single and a double membrane type hydrophone. While the double membrane type shows an overall higher sensitivity, it also exhibits a substantial directionality, in particular around the resonance peaks. We converted the measured wavelength shift pressure sensitivity for a direct comparison with ambient sea state noise. It was found that the sensitivity of the technology is between sea state 0 and 1 for most of the dynamic range, which allows for detecting weak acoustic signals generated by neutrino interactions in the deep sea.

Measurements on pulses show the impact of a complex transfer function. As expected, transient signals exhibit significant ringing. However, after deconvolution of the fiber hydrophone response the pulse shape matches the reference pulse, confirming that the transfer function is well-characterized and can be corrected. As the pulse shape and size is directly related to the energy of the interacting neutrino, deconvolution is important. Various approaches can be employed, including the deconvolution method presented here, system identification techniques, or even convolution of a template bank with the hydrophone response in the context of matched

filtering. The discussion on how the deconvolution exactly is carried out once the hydrophones are implemented in a full size neutrino telescope is beyond the scope of this paper.

Pressure qualification has been carried out to confirm the working principle of the static pressure compensation mechanism. The hydrophone was put in a vessel whereafter a pressure of 140 bar (14 MPa) was applied. The hydrophone showed no degradation in sensitivity after the pressure cycle. Transient signals that were observed during the pressure qualification showed that the mechanical resonance of the transducer did not change prior, during and post qualification. This may lead to the conclusion that the transfer function of the transducer under pressure is similar to the one outside the pressure vessel. Whether the overall sensitivity changes under pressure needs verification in a dedicated experiment. It requires an acoustic set-up in a high pressure environment.

Finally, we have investigated some aspects that are related to the integration of the transducer that might have an impact on the transfer function. The impact of a protective cap on the acoustic performance of the transducer has been investigated and it has been shown that the mechanical eigenresonance is affected. Then, the effect on residual air has a substantial impact on the performance of the transducer by shifting the resonance frequency to lower values and increasing the sensitivity at lower frequencies. It should be noted that when the hydrophone is operated in deep sea, all airbubbles will be squeezed out due to the ambient pressure.

The concept of distributed sensing using optical fibers combined with the results of the acoustic measurements and the pressure qualification makes the technology is well suited for the implementation in a large acoustic neutrino telescope.

7. Acknowledgement

This research was funded by NWO, project nr 184.034.013.

8. Bibliography

- [1] G.A. Askaryan. Hydrodynamic radiation from the tracks of ionizing particles in stable liquids. *The Soviet Journal of Atomic Energy*, 3(2):921 – 923, 1957.
- [2] G.A. Askaryan, B.A. Dolgoshein, A.N. Kalinovsky, and N.V. Mokhov. Acoustic detection of high energy particle showers in water. *Nuclear Instruments and Methods*, 164(2):267–278, 1979.
- [3] J.G. Learned. Acoustic radiation by charged atomic particles in liquids: An analysis. *Phys. Rev. D*, 19:3293–3307, Jun 1979.
- [4] S. Bevan, S. Danaher, J. Perkin, S. Ralph, C. Rhodes, L. Thompson, T. Sloan, and D. Waters. Simulation of ultra high energy neutrino induced showers in ice and water. *Astroparticle Physics*, 28(3):366–379, 2007.
- [5] Clara Gatus Oliver. Acoustic signals from ultra high energy cosmic neutrinos. Master’s thesis, University of Amsterdam, 2020.

- [6] E. J. Buis, E. J. J. Doppenberg, R. A. Nieuwland, and P. M. Toet. Fibre laser hydrophones for cosmic ray particle detection. *JINST*, 9:C03051, 2014.
- [7] Ernst-Jan Buis, Ed Doppenberg, Robert Lahmann, and Peter Toet. A large fiber sensor network for an acoustic neutrino telescope. *EPJ Web Conf.*, 135:06006, 2017.
- [8] A.D. Kersey. A review of recent developments in fiber optic sensor technology. *Optical Fiber Technology*, 2(3):291–317, 1996.
- [9] V.O Knudsen, R.S. Alford, and J.W. Emling. Underwater ambient noise. *Journal of Marine Research*, 7(2):410–429, 1948.
- [10] R.J. Urick. *Principles of Underwater Sound*. McGraw-Hill, 1983.
- [11] J.R. Short. High-frequency ambient noise and its impact on underwater tracking ranges. *IEEE Journal of Oceanic Engineering*, 30(2):267–274, 2005.